SpezialForschungsBereich F 32

Karl–Franzens Universität Graz
Technische Universität Graz
Medizinische Universität Graz

Reconstruction artefacts in magnetic induction tomography due to patient's movement during data acquisition

Doğa Gürsoy Hermann Scharfetter

SFB-Report No. 2008–011 September 2008

A–8010 GRAZ, HEINRICHSTRASSE 36, AUSTRIA

Supported by the
Austrian Science Fund (FWF)

SFB sponsors:

- **Austrian Science Fund** (FWF)
- **University of Graz**
- **Graz University of Technology**
- **Medical University of Graz**
- **Government of Styria**
- **City of Graz**

Reconstruction artefacts in magnetic induction tomography due to patient's movement during data acquisition

Doğa Gürsoy and Hermann Scharfetter

September 1, 2008

Abstract

Magnetic Induction Tomography (MIT) attempts to obtain the distribution of passive electrical properties inside the body. Eddy currents are induced in the body using an array of transmitter coils and the magnetic fields of these currents are measured by receiver coils. In clinical usage, the relative position of the coils to the body can change during data acquisition because of the expected/unexpected movements of the patient. Especially in respiration monitoring these movements will inevitably cause artefacts in the reconstructed images. In this paper, this effect was investigated for both state and frequency differential variants of MIT. It was found that a slight shift of the body in the transverse plane causes spurious perturbations on the surface. In reconstructions, this artefact on the surface propagates towards the center in an oscillatory manner. It was observed that the movement can corrupt all the valuable information in state differential MIT, while frequency differential MIT seems more robust against movement effects. A filtering strategy is offered in order to decrease the movement artefacts in the images. To this end, monitoring of the patient's movement during data acquisition is required.

Keywords: Magnetic induction tomography, image reconstruction, movement artefacts

1 Introduction

MIT is a contactless imaging modality which aims to reconstruct the conductivity distribution of the body (see eg Griffiths 2001, Korjenevsky 2000, Peyton

[1]D. Gürsoy and H. Scharfetter are with the Institute of Medical Engineering, Graz University of Technology, Austria. e-mail: guersoy@tugraz.at

[2]This work was supported by the SFB project F32-N18 granted by the Austrian Science Fund and will be published in IOP Physiological Measurements.

1996, Tapp 2003). Eddy currents are induced in the body by an array of transmitter coils and the magnetic field of these currents are measured by receiver coils. In practice, because of the high sensitivity of the MIT system to the noise and the nonlinearity of the forward operator, the perturbations around a reference conductivity distribution have commonly been used. Usually, a uniform phantom is used to obtain the reference voltage data, however, nonuniform phantoms may also be used. The idea is to identify only the changes in conductivity distribution by taking a reference which resembles expected values (eg conductivities of healty person tissues or uniform background conductivity).

The variants of MIT can be classified into two categories depending on the selection of the reference. The first one is the state differential MIT, in which the reconstructions are formed by taking a reference state using *a priori* knowledge of the model conductivity distribution. Possible applications may include respiration monitoring (Sapetsky and Korjenevsky 2004), oedema imaging (Merwa 2004) or monitoring of tumour development. The second category is frequency differential MIT (Brunner 2006) which uses the fact that the conductivity profile of the tissues are dependent on the operating frequency of the excitation field. In frequency differential MIT, the reference data is obtained at a different operating frequency than the measurement dataset. Imaging of motionless organs like brain or pelvis seems more appropriate with this modality.

In all the applications of MIT, the body can move during the data acquisition and this affects the reconstructed images. Especially for thorax applications this movement is inevitable unless a breath hold protocol during imaging is feasible. Therefore, in this paper, the effect of the patient's movement during data acquisition to the reconstructed images was determined and then some possible solutions are proposed to compensate this effect.

The same problem exists in electrical impedance tomography (EIT) (Zhang and Patterson 2005). In EIT, the sensors are attached to the surface and this automatically roughly maintains the relative position of the body to the sensors. However, in MIT the effect is more dominant on the surface of the body because the sensors are usually fixed in space and a slight shift of the body can cause a significant position change with respect to the coils.

In this paper, the coil geometry of a spectroscopic 16 channel MIT system is used for simulations. To model the movement effects, we changed the position and shape of the body with respect to a reference model and we tried to reconstruct spherical inhomogeneities inside a cylindrical container for both state and frequency differential MIT. The simulations were also conducted for 20 dB SNR level to test the stability of the inversion. To overcome the movement effect, possible preprocessing and postprocessing solutions based on a filtering strategy were discussed.

2 Methods

2.1 Simulation of the voltage data

The relation of the voltage data and the electrical properties is expressed as a nonlinear forward operator,

$$v = \psi(\kappa) \tag{1}$$

where $\kappa = \sigma + jw\epsilon$ is defined as the complex conductivity.

To solve for the voltages, the fields in the body must be solved given the primary magnetic vector potential via transmitter coils. For biological applications of MIT, it is usually assumed that the contribution of the induced currents to the primary magnetic potential to be negligible. This results in decoupling of the field equations (see eg Gençer 1999). Therefore, the magnetic potential distribution calculated (Smythe 1965) in the absence of a conducting body is used for the solution of the electric scalar potential with the body present. The resulting time harmonic partial differential equations for the solution of the scalar potential in the body are given as folows,

$$\nabla \cdot \kappa \nabla \phi = -jw\mathbf{A} \cdot \nabla \kappa \tag{2}$$

$$\frac{\partial \phi}{\partial n} = -jw\mathbf{A} \cdot \mathbf{n} \tag{3}$$

where w is the angular operating frequency of the excitation field, ϕ and $\mathbf{A}$ are the electric scalar and magnetic potentials and $\mathbf{n}$ is the normal vector directed outward from the body surface. The equation set was discretisized by the Finite Element Method and solved by the inverse based multilevel preconditioned quasi minimum residual method (Horesh 2006). Using the solved potentials, the electric field in the body was found by,

$$\mathbf{E} = -\nabla \phi - jw\mathbf{A} \tag{4}$$

The electric field in the body generates secondary magnetic field which was calculated from the Biot-Savart law,

$$\mathbf{B} = \frac{\mu_0}{4\pi} \int \kappa \mathbf{E} \times \frac{\mathbf{r}}{r^3} dV \tag{5}$$

where $\mathbf{r}$ is the displacement vector in the direction pointing from the element towards the point at which the field is being computed and the integration is taken over the volume of the body. In MIT, the measured quantity is the voltages induced in the receiving coils because of the existing magnetic field. The voltage signal can be subdivided into two parts due to the influence by the primary and the secondary magnetic field. The first one is independent of the electrical properties and the cancellation of that signal from the data is usually desired. Possible ways of cancellation are using gradiometers, back off coils or lateral positioning of receivers. In this paper, it was assumed that a perfect cancellation of the primary signal was established. Therefore the

induced secondary voltages in the receiver coils were found using Lenz's Law by integrating the magnetic field over the receiver coil surfaces,

$$v = -jw \int \mathbf{B} \cdot d\mathbf{S} \tag{6}$$

The coupling between the real and imaginary components was assumed to be negligible. Thus, the real part of the voltage data (in-phase component with respect to the primary excitation) contains conductivity information and the imaginary part contains the permittivity information of the body. The aim is to reconstruct conductivity distribution, therefore, only the real component was used for imaging.

For the realistic simulations, an additive noise of 20 dB was added to the data. The noise was assumed to be independent of the data and taken as gaussian, $N(0, n^2)$, where n^2 is the variance of the noise distribution. SNR is defined as,

$$SNR = 10\ log\left(\frac{\Delta v_{max}^2}{n^2}\right) \tag{7}$$

where Δv_{max} is the maximum secondary voltage difference between the data sets obtained by the perturbed model and the reference. 100 random samples of the gaussian noise distribution was formed to realize the noise.

2.2 Linearization

ψ is a nonlinear function and usually a linearization of this operator is possible around a given σ_o assuming σ_o is in the close vicinity of the expected body parameters. This linear relation is expressed as,

$$\frac{\partial \psi(\sigma_o)}{\partial \sigma} \Delta\sigma = \Delta v \tag{8}$$

In MIT context, the Jacobian of the forward operator at a given conductivity distribution is usually named the sensitivity and the discretisized linear relationship is written as follows,

$$\mathbf{S}_o \Delta\sigma = \Delta v \tag{9}$$

by denoting $\mathbf{S}_o$ as the sensitivity matrix for a given σ_o. The sensitivity matrix was calculated by the adjoint approach using the generalized version of Geselowitz's relationship (Mortarelli 1980) which is generally used for EIT sensitivity calculations based on the reciprocity theorem. It is defined in terms of the inner product of the current density in the body and the adjoint electric field,

$$\mathbf{s}_k = \int (\Delta\sigma \mathbf{E}_i) \cdot \mathbf{E}_j dV \qquad k = 1, 2, .., n \tag{10}$$

where $\mathbf{E}_i$ is and $\mathbf{E}_j$ corresponds to the electric fields created by the normal and adjoint excitations of the transmitter and receiver coils respectively and n is the number of independent measurements. s_k denotes the k^{th} row of the sensitivity matrix. The integration is taken over the volume of the body.

2.3 Image reconstruction

By applying the least squares approximation (to eqn 9) and minimizing the error, the conductivity distribution can be obtained from,

$$\Delta\sigma = (\mathbf{S}_o^T\mathbf{S}_o)^{-1}\mathbf{S}_o^T\Delta v \tag{11}$$

where $\mathbf{S}_o^T\mathbf{S}_o$ is an approximation of the Hessian of the forward operator for a given σ_o. Due to the computational errors and low number of data channels, the Hessian matrix is usually ill-posed and needs regularization in the presence of data inaccuracies. A strong singularity arises because of the fact that some of the eigenvalues of the Hessian matrix are very small which causes a strong amplification of the errors in the conductivity domain.

The MIT problem is very underdetermined, therefore, using the following equivalent expression (by applying Woodbury identity) was preferred,

$$\Delta\sigma = \mathbf{S}_o^T(\mathbf{S}_o\mathbf{S}_o^T)^{-1}\Delta v \tag{12}$$

Similarly $\mathbf{S}_o\mathbf{S}_o^T$ is usually singular and an additional term of the form $\lambda\mathbf{R}$ is added for the compensation of noise where $\mathbf{R}$ is the regularization matrix and λ is the regularization parameter. In this study $\mathbf{R}$ was chosen as the identity matrix and λ was obtained according to the Morozov criterion (Hansen 1998).

2.4 Model

A cylindrical phantom (0.1 S/m) which has 4 spherical inhomogeneities (0.2 S/m) was used for simulations (see Figure 1). The phantom had a radius of 100 mm and a height of 200 mm. The inner perturbations had a radius of 20 mm and were positioned at (-60,0,0), (60,0,0), (0,60,0) and (0,-60,0) mm. The tetrahedral mesh was formed by the commercial software HyperMesh (Altair Inc.). The total element number was ∼450 000 for simulating the data (forward model) and ∼150 000 for the image reconstructions (inverse model).

The transmitter and receiver coil pairs encircle the phantom positioned in a zigzag arrangement. The two coils in front of a transmitter were connected in counterphase to form a gradiometer. The reference data were simulated with the conductivity of the spheres set to 0.1 S/m, the same as the background. The voltage data were simulated with the conductivity of the spheres raised to 0.2 S/m, as if the spheres were dispersive and that the second voltage set had been gathered at a higher frequency. The permittivity was taken as 80 in the whole phantom.

2.5 Movements

The body movement was simulated both as a shift (along -x direction from the reference position) to model the unexpected movements and as a uniform radial expansion to model the respiration artefacts (figure 2). 2 mm and 4 mm of shifts/expansions were chosen which corresponds to 10% and 20% change in the

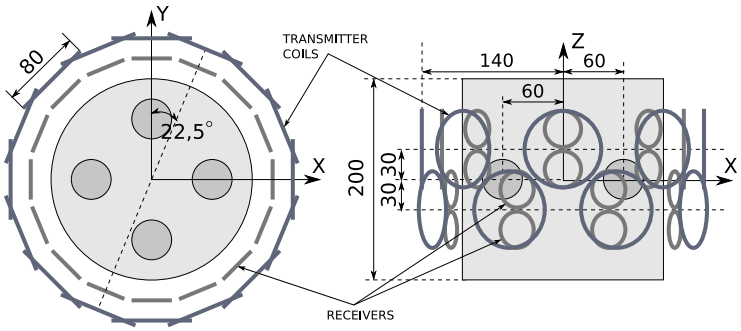

Figure 1: Simulation arrangement for solving the inverse problem and generating simulated voltage data: (left) top view, (right) side view. All measures are in mm.

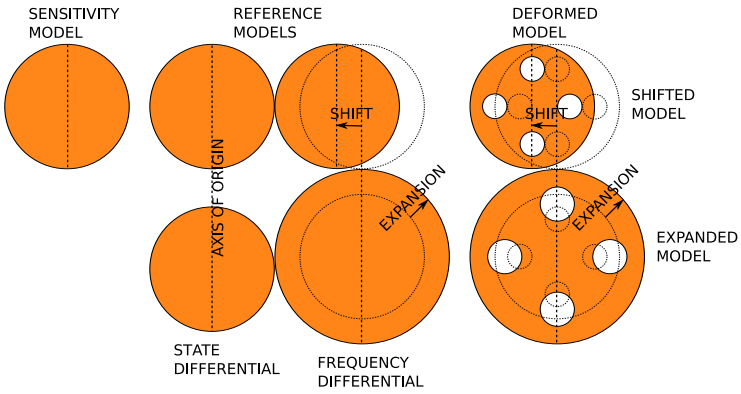

Figure 2: Modelling of body movements. Shift from the original position were chosen as 2 and 4 mm which corresponds to 10% and 20% change in the distance between the surface of the phantom and the receivers. All movements are assumed to be on transversal plane

distance between the surface of the phantom and the receivers. In state differential simulations the reference and voltage data were assumed to be taken in different times, which may result in geometrical inconsistencies between the states. Therefore the reference was taken as the original configuration and the voltage data was obtained from the geometrically distorted model. However, in frequency differential simulations, the reference and voltage data were assumed to be taken simultaneously, as a snapshot. Thus, the reference data was also taken from the homogenous but distorted model. The sensitivity matrix had been computed for the original state assuming a zero information of the movement/distortion.

2.6 Evaluation

The image quality was quantitatively compared by calculation of the Pearson product-moment correction coefficient (PMCC) between the images with and without the geometrical distorsion for different types of body movement to indicate the strength of linear relationship between them. PMCC for the two reconstructions $\Delta\sigma_1$ and $\Delta\sigma_2$ is defined as,

$$PMCC_{\Delta\sigma_1,\Delta\sigma_2} = \frac{\sum x_i y_i - n\bar{x}\bar{y}}{(n-1)s_x s_y} \tag{13}$$

where $\bar{x}$ and $\bar{y}$ are the sample means of $\Delta\sigma_1$ and $\Delta\sigma_2$, s_x and s_y are the sample standard deviations of $\Delta\sigma_1$ and $\Delta\sigma_2$ and n is the number of voxels in the inverse mesh.

2.7 Filtering

It was observed that the image obtained in the presence of movement is a linear combination of the movement artefacts and the undistorted image. Therefore if the geometrical distortions of the body surface is measured in terms of expansion and shifts/rotation, the geometrical modelling errors can be filtered out by subtracting the simulated data of the distorted uniform model from the raw data before the image reconstruction process (prefiltering). It is also possible to filter out the effects after the image reconstruction process (postfiltering) similarly by subtracting the images obtained by using the simulated data and real data, however, the latter one is more time consuming and will only be used for visualizing/understanding the filter behaviour. For practical purposes prefiltering is more suitable since it requires only one inversion instead of two inversions.

3 Results

The images were reconstructed for different types of movements using the simulation arrangement which is given in figure 1. State and frequency differential

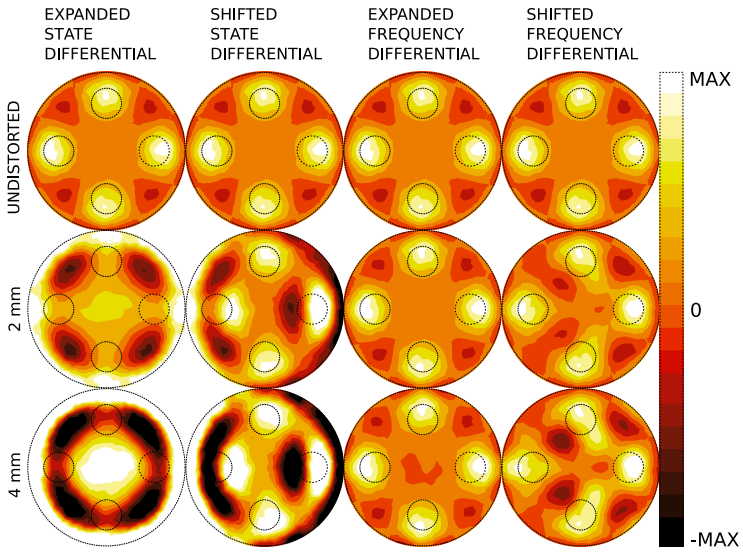

Figure 3: Noise free reconstructions.

MIT reconstructions for different degrees of shift in x direction and radial expansion were given on figure 3. The colorbar is the same for all images and *max* denotes the maximum conductivity value of the undistorted reconstructions when no shift or expansion were present (upper row). For the state differential images, strong positive and negative artefacts arose at those surface regions which experience the largest change of normal distance with respect to the coils. This artefact on the surface propagated towards the center in an oscillatory manner. In frequency differential images the perturbations appear partly displaced and ghosts appear/shift especially near/towards the central region. However, no considerable artefacts were noted in the images of radially expanded models. While in the frequency differential images the perturbations can be identified even at comparatively strong distorsions, this is hardly possible in the state differential images.

The simulations with 20 dB noise added to the data are presented in figure 4. With noisy data, excessive values of conductivity were observed on the surfaces of the phantom in the state differential images and the artefacts propagated towards the center in an oscillatory manner similarly. While this artefact heavily corrupted the state differential images, the frequncy differental images were more stable and the perturbations were identified clearly. In addition, in frequency differential images, no unsymmetrycal artefacts due to the movement were noticed.

The inversion reconstructs the geometrical distortions as well as the internal inhomogeneities. However, the high reconstructed conductivity values near the surface are dominating depending on the fact that the resolution is getting low

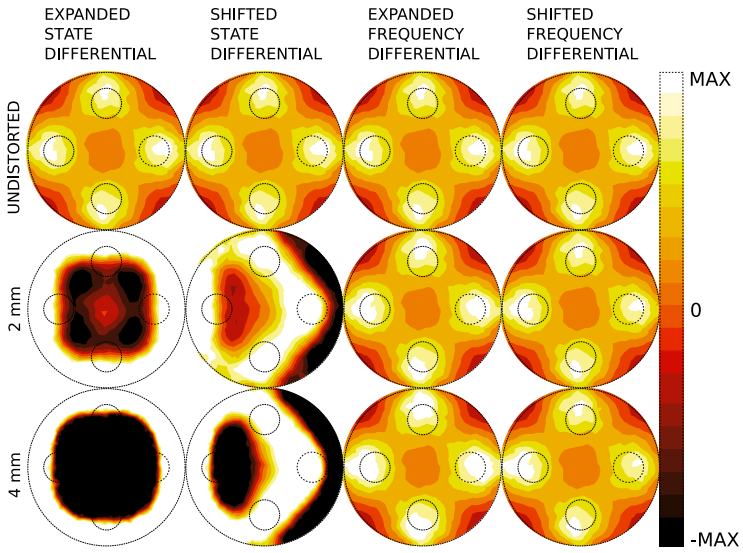

Figure 4: Reconstructions with 20 dB noise.

in central regions. The oscillatory behaviour and ghosts in images are expected and caused by the *sinc* like point spread functions (Merwa 2007).

The PMCC between the undistorted image and the images which were obtained with different types of movements during data acquisition are plotted in figure 5. The frequency differential images were significantly higher correlated than the state differential images. A moderate almost linear decay of PMCC for up to 6 mm of shifts (or change of shape) was observed in the frequency differential case. However, in the state differential case, there is a strong approximately exponential decay of the PMCC already at small distorsions.

4 Discussions

In frequency differential MIT, the data acquisition for different states is done simultaneously. This is accomplished by excitation of the body with two or more different frequencies at the same time. On the other hand in state differential MIT, the measurements between different states are taken at different times. Naturally, it is more probable to observe unwanted changes of the shape and position of the body between the states. Simulations confirmed that in state differential MIT, usually the reconstructed images are either very poor or totally corrupted when body movement is present, however, frequency differential MIT is more stable to body movement effects.

In EIT, a similar discussion concerning movement effects was done (Zhang and Patterson 2005). However because of the static nature of the receivers, in MIT, this movement effect is expected to be much stronger than EIT. Therefore

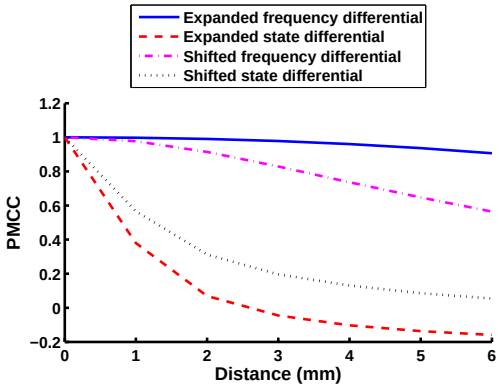

Figure 5: PMCC between the undistorted image and the images which were obtained with different types of movements during data acquisition.

we believe that this is one of the major problems in MIT, especially in thorax monitoring.

It was observed that the image obtained in the presence of movement is a linear combination of the movement artefacts and the undistorted image. Therefore, if the exact position and the shape of the model during data acquisition is known, it may be possible to compensate the movement artefacts to some degree. By using the surface information, simulating the movement effect using a uniform phantom and subtracting this from the reconstructed image would remove the movement artefacts (see figure 6). Similarly, one can do the same process in the voltage data before reconstruction by subtracting the simulated data from the actual data when the uniform phantom is moved. To monitor the movement, one possibility is to use a camera system working synchronized with the data acquisition system (see eg. Tapp 2003). Similarly, cheaper solutions like ultrasonic distance sensors may also be used.

The results indicate that frequency differential MIT is more promising, especially for thorax applications. However we must emphasize that our analysis is valid only for local inhomogeneities in a non-dispersive background. Preliminary results with realistically simulated respiration data, however, yield comparatively poor images. The reason may be the fact that in frequency differential MIT the electrical properties of the background also change between the states and the inversion algorithms so far developed have not been tested with data from object with a dispersive background. An illustration of this drawback is given on figure 7. The voltage data for both images was simulated by changing the conductivity of the spherical perturbations from 0.1 S/m to 0.2 S/m. A constant background conductivity of 0.1 S/m was assigned to the left phantom. However the right phantom was modelled to have a dispersive background (a conductivity change of the background from 0.1 S/m to 0.15 S/m between

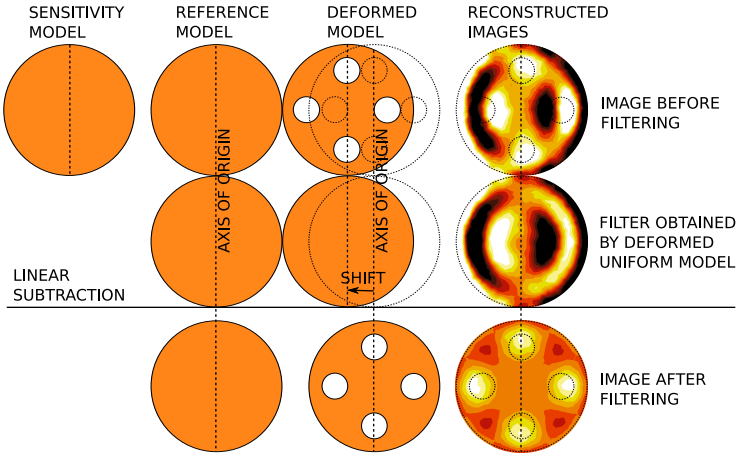

Figure 6: Illustration of the filtering strategy used to remove movement artefacts.

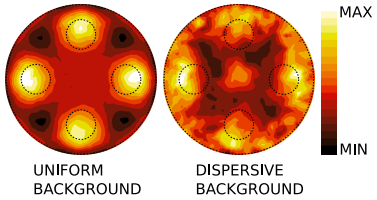

Figure 7: The frequency differential images obtained by assigning the (left) same and (right) different conductivity values to the background for seperate states of data simulation.

states). The resulting resonstructions show the incapability of the linearized inversion algorithm due to the dispersive medium. We think this is one of the biggest challenges in frequency differential MIT.

This paper considers only the movement of the body as a whole and does not consider the individual movements of interior inhomogeneities. The latter would be the case when the heart and lungs moved in different directions and their shape changed independently during respiration/heartbeat cycles. The proposed solutions based on pre/postfiltering which rely on a measurement of the position of the surface of the body with respect to the coils still cannot solve the latter problem. Future work should aim at modeling and simulating all these movements and search for possible solutions to reduce the image artefacts.

5 Acknowledgments

The authors thank Olaf Steinbach, Institute of Numerical Mathematics, Graz University of Technology, as the main partner concerning mathematical issues within the subproject. This cooperation and many fruitful discussions with Manuel Freiberger, Sarah Engleder and Sabine Zaglmayr are gratefully acknowledged.

References

[1] Brunner P, Merwa R, Missner A, Rosell J, Hollaus K and Scharfetter H 2006 Reconstruction of the shape of conductivity spectra using differential multi-frequency magnetic induction tomography *Physiol. Meas.* **27** 237-48

[2] Gençer N G and Tek M N 1999 Electrical conductivity imaging via contactless measurements *IEEE Trans. Med. Imag.* **18** 617-27

[3] Griffiths H 2001 Magnetic Induction Tomography *Meas. Sci. Technol.* **26** 1126-31

[4] Hansen P 1998 *Rank-Deficient and Discrete Ill-Posed Problems* (Philadelphia: SIAM)

[5] Horesh L, Schweiger M, Bollhofer M, Douiri A, Holder D S and Arridge S R 2006 Multilevel preconditioning for 3D large scale soft field medical applications modeling *Int. J. Inf. Syst. Sci.* **2** 532-56

[6] Korjenevsky A, Cherepenin V and Sapetsky S 2000 Magnetic induction tomography: experimental realization *Physiol. Meas.* **21** 8994

[7] Merwa R, Hollaus K, Biro O and Scharfetter H 2004 Detection of brain oedema using magnetic induction tomography: a feasibility study of the likely sensitivity and detectability *Physiol. Meas.* **25** 347-54

[8] Merwa R and Scharfetter H 2007 Magnetic induction tomography: evaluation of the point spread function and analysis of resolution and image distortion *Physiol. Meas.* **28** 313-24

[9] Mortarelli J R 1980 Generalization of the Geselowitz Relationship Useful in Impedance Plethysmographic Field Calculations *IEEE Trans. Biomed. Eng.* **27** 665-7

[10] Peyton A 1996 An overview of electromagnetic inductance tomography: description of three different systems *Meas. Sci. Technol.* **7** 261-71

[11] Sapetsky S A and Korjenevsky A V 2004 Magnetic induction tomography: visualization of extensive objects *Proc. 12th Int. Conf. Electrical Bio-Impedance and 5th Electrical Impedance Tomography*, 696-8

[12] Smythe W R 1965 *Static and dynamic electricity*, (New York: McGraw Hill) 290-1

[13] Tapp H S, Goss D, Mackin R O, Crescenso E, Wan-Daud W A, Ktistis C and Peyton A J 2003 A combined digital camera: EMT system to measure human body composition, *3rd World Congress on Industrial Process Tomography*, 384-90

[14] Zhang J and Patterson R P 2005 EIT images of ventilation: what contributes to the resistivity changes? *Physiol. Meas.* **26** 81-92